Histol Histopathol (2022) 37: 1201-1212

http://www.hh.um.es

Histology and Histopathology
From Cell Biology to Tissue Engineering

ORIGINAL ARTICLE **Open Access**

Tumors derived from lung cancer cells respond differently to treatment with sodium valproate (a HDAC inhibitor) in a chicken embryo chorioallantoic membrane model

Raminta Diržiuvienė[1], Lina Šlekienė[1], Jolita Palubinskienė[1], Ingrida Balnytė[1], Kristina Lasienė[1], Donatas Stakišaitis[1,2] and Angelija Valančiūtė[1]

[1]Department of Histology and Embryology, Medical Academy, Lithuanian University of Health Sciences, Kaunas and [2]Laboratory of Molecular Oncology, National Cancer Institute, Vilnius, Lithuania

Summary. Lung cancer is the most frequent cause of cancer death. Some human lung malignant tumors have a combined small-cell lung cancer (SCLC) and non-small-cell lung cancer (NSCLC) histology, with tumor cell phenotype changing during tumor progression. Valproic acid is used as an anti-seizure medication to treat migraine, and bipolar mood disorders. Recently, its efficacy as an adjuvant therapy was shown in cancer due to its histone deacetylase (HDAC) inhibitory property. HDACs are upregulated in lung tumors, and HDAC inhibitors, including valproic acid, inhibit endothelial cell proliferation *in vitro* and *in vivo* and have antiproliferative and antimigratory properties. We tested valproic acid for possible antiangiogenic and antimigratory effects on experimental lung tumors grafted onto the chicken embryo chorioallantoic membrane (CAM). Tumors were formed from two NSCLC cell lines and a single SCLC cell line. To investigate tumor and CAM interactions, *in vivo* biomicroscopy, visualization of blood vessels with injected fluorescent dextran, histological, immunohisto-chemical and histomorphometric methods were applied. Our results showed that a sodium valproate (NaVP) treatment-induced a dose-dependent decrease of experimental tumor invasion into the CAM mesenchyme and a reduction in angiogenesis. Both the invasion and the angiogenic response were dependent on the type of cell line used: invasion and angiogenesis of tumors derived from A549 and NCI-H146 cell lines responded to increasing doses of NaVP from 4 to 8 mM, whereas Sk_Lu_1 cells response were antimigratory and antiangiogenic when NaVP was used up to 6 mM. When 8mM NaVP was used, stimulated invasion and angiogenesis in tumors from Sk_Lu_1 cells were observed.

Key words: Lung cancer, A549, Sk_Lu_1, NCI-H146, Sodium valproate, Chicken chorioallantoic membrane, Histone deacetylase

Corresponding Author: Raminta Diržiuvienė, Department of Histology and Embryology, Medical Academy, Lithuanian University of Health Sciences, Mickevičiaus str. 9, Kaunas, Lithuania, e-mail: raminta.dirziuviene@lsmu.lt

DOI: 10.14670/HH-18-482

Introduction

Lung cancer is the most frequent cause of cancer death (Oser et al., 2015). According to the World Health Organization classification, there are two main histological subtypes of lung cancer: non-small-cell lung cancer (NSCLC), accounting for about 85% of cases, with the remaining 15% of cases being small-cell lung cancer (SCLC). Adenocarcinoma, squamous-cell carcinoma, and large-cell carcinoma, belong to NSCLC (Oser et al., 2015; Vos et al., 2016). Lung cancer treatment decisions are based on expectations that a patient's cancer is entirely of one subtype (Kalemkerian et al., 2013), but some lung malignant tumors have combined SCLC and NSCLC histologies (Adelstein et

Abbreviations. NSCLC, non-small cell lung cancer; SCLC, small-cell lung cancer; VEGF, vascular endothelial growth factor; CAM, chicken chorioallantoic membrane; HDAC, histone deacetylase; NaVP, sodium valproate; EDD, embryonic day of development; A549, lung cancer cell line; Sk_Lu_1, lung cancer cell line; NCI-H146, lung cancer cell line; RPMI, Roswell Park Memorial Institute; HEPES, 4-(2-hydroxyethyl)-1-piperazineethanesulfonic acid; FBS, fetal bovine serum; EMEM, Eagle's Minimum Essential Medium; H+E, haematoxylin and eosin; αSMA, alpha smooth muscle actin; NaDCA, sodium dichloroacetate; VGSCs, voltage-gated sodium channels; HER2, human epidermal growth factor receptor 2.

al., 1986; Mangum et al., 1989). In cases of combined histologies or when repeated biopsies show a transformation from one type to another, treatment decisions are difficult (Sequist et al., 2011; Yu et al., 2013; Bar et al., 2019).

Tumor progression is associated with increased vascularization, where malignant cells are located close to blood vessels for access to oxygen and nutrients that are essential for proliferation and invasion. Tumors induce and attract new blood vessels from surrounding tissues via numerous molecular mechanisms (Kuczynski et al., 2019). The concept that tumor progression is associated with angiogenesis was formulated in 1971 (Folkman, 1971; Folkman et al., 1971). Since then, various antiangiogenic strategies have been tested in experimental and preclinical research. Despite promising results in preclinical studies, antiangiogenic strategies are not beneficial in all tumor types (Vasudev and Reynolds, 2014). The vascular endothelial growth factor (VEGF) pathway is the most important regulator of tumor neovascularization (Carmeliet et al., 2005). Angiogenesis also plays an important role in both SCLC and NSCLC. It is also worth noting that SCLC has a higher vascularization compared to NSCLC (Lucchi et al., 2002).

Our research investigated the possible antiangiogenic and antimigratory effects of valproic acid in experimental lung tumors grafted onto the chicken embryo chorioallantoic membrane (CAM). Our hypothesis was based on previous studies that showed that histone deacetylase (HDAC) inhibitors, including valproic acid, can inhibit endothelial cell proliferation *in vitro* and *in vivo* (Michaelis et al., 2004; Iizuka et al., 2018). Valproic acid may also diminish these endothelial responses to VEGF (Iizuka et al., 2018). Since valproic acid is used for the treatment of epilepsy, its pharmacological activity, toxicity and interactions with conventional chemotherapy have been well characterized (Hubaux et al., 2015). To investigate cancer-induced angiogenesis and the antiangiogenic potential of valproic acid in an experimentally derived tumor, we used an established CAM model. It is known that the CAM is formed after embryonic day of development 5 (EDD5) by partial fusion of the chorion and the allantois, and by EDD12 the CAM completely surrounds the whole embryo (Melkonian et al., 2002). Importantly for this study, it is a highly reproducible *in vivo* model, in which it is easy to access the experimental tumor and inspect any induced angiogenesis via an open window in the eggshell. This research tested the effect of different doses of sodium valproate (NaVP) on angiogenesis and quantified of several CAM parameters such as blood vessel density and CAM thickness. In addition, the CAM model was used to study cancer invasion since the basement membrane of the chorionic epithelium resembles the human epithelial barrier (Schmitd et al., 2019). We showed that the CAM model could be used to further study the pharmacodynamics of drugs that regulate tumor microenvironment, angiogenesis, and cancer invasion. Experimental tumors used in this study were formed from three different lung cancer cell lines: A549, NSCLC derived from a 58 -year-old Caucasian male; Sk_Lu_1 NSCLC derived from a 60 -year-old Caucasian female; and NCI-H146 SCLC derived from a 59 -year-old white male. All cell lines formed tumors, which were treated with different doses of NaVP.

Materials and methods

The investigated objects

To determine the antitumor and antiangiogenic effect of NaVP, experimental tumors were formed from cells derived from three different lung cancer cell lines (A549, Sk_Lu_1, and NCI-H146) and grafted onto the surface of the CAM, after each was treated with 4, 6 or 8 mM of NaVP. Thus, there were nine experimental groups in total. The control groups consisted of tumors formed from respective cell lines without any treatment applied before the grafting. Blood vessel number per constant length (1792.52 μm) and thickness of the CAM under the tumor were determined in CAMs, also in the ones without any tumor nor treatment applied and these were regarded as intact control. The total number of investigated objects is presented in Table 1.

Cell culture

Human Small Cell Lung Cancer NCI-H146 cells were obtained from the State Research Institute Centre for Innovative Medicine (Vilnius, Lithuania). Non-Small Cell Lung Cancer A549 cells were kindly provided by the University of Bialystok, Poland and NSCLC cells Sk_Lu_1 were purchased from The Global Bioresource Center (ATCC, USA). The NCI-H146 and A549 cells were placed in 75 cm^2 tissue culture flasks and maintained in RPMI 1640 medium (Sigma-Aldrich, USA) supplemented with 4.5 g/L glucose, 2 mM L-glutamine, sodium pyruvate (Gibco, USA), HEPES 10% heat-inactivated fetal bovine serum (FBS). 100 U/ml penicillin and 100 μg/ml streptomycin (Lonza, Belgium). EMEM media was enriched with calcium bicarbonate of 1500 mg/L in addition to previously described media supplements and was used to cultivate Sk_Lu_1 cells. All cells were grown at 37°C in a humidified chamber containing 5% CO_2. The medium

Table 1. Number of investigated objects.

	Experimental (n)			Control (n)	Control CAM
	4mM NaVP	6mM NaVP	8mM NaVP	With tumor	Without tumor
A549	11	10	10	12	15
Sk_Lu_1	11	13	12	15	
NCI-H146	16	14	18	25	

was routinely changed every 2 to 3 days after seeding. Trypsin (0.05%, Gibco, USA) was used to resuspend A549 and Sk_Lu_1 cells. Formed clusters were collected by centrifugation and resuspended in a fresh medium.

Tumor xenograft model

Cells suspensions were centrifuged and the, supernatant removed, before resuspension with solutions of 4 mM, 6 mM or 8 mM NaVP (Sigma Aldrich; Merck KGaA, USA) dissolved in serum-free RPMI-1640 medium and rat tail collagen type I (Gibco, USA) to a final concentration of approximately $1x10^6$ cells/20 µl. Control tumors were formed in the same manner but without NaVP 20 µl cell suspensions were pipetted onto an absorbable sponge (SURGISPON®, Aegis Lifesciences, India) (2.5x2.5x1 mm) to make a solid form, which was then placed onto the CAM surface on the 7^{th} day of egg incubation, EDD7.

Chorioallantoic membrane (CAM) assay

Fertilized Cobb 500 chicken eggs from a local hatchery were transferred into a hatching incubator (Maino incubators, Oltrona S.M. Co, Italy) that was equipped with an automatic humidifier (Maino Enrico, R1569, Italy) and rotator. According to European law (Directive 2010/63/EU of the European Parliament and of the Council of 22 September 2010 on the protection of animals used for scientific purposes) and order of the Lithuanian State Food and Veterinary Service Directive (No. B1-866 of 16 October 2012) experiments with chicken embryo do not raise any ethical or legal concerns and do not require special permission. Relative air humidity was 60% and the temperature was set at 37.7°C. Eggs were automatically rotated until EDD3. On EDD3, a small hole at the air chamber end of the egg was drilled into the shell, with approximately 2 ml of albumin removed before being sealed with sterile taped. Then, a window in the eggshell of approximately 1 cm in diameter was drilled and removed, before being covered once again with sterile transparent tape. The eggs with a developing embryo were then returned to the incubator with rotation turned off. All eggs were kept in the incubator under the same conditions until the grafting of tumors and the harvesting of the CAM.

In vivo biomicroscopy

Eggs with formed tumors were inspected daily *in ovo* from Day 2 to Day 5 post-grafting (equivalent to EDD 9-12) under a stereomicroscope (OLYMPUS SZX16, Japan) equipped with an Olympus DP72 digital camera and photographed using CellSens Dimension 1.9 Digital Imaging Software. On EDD12 10 µl of fluorescent dextran (Sigma-Aldrich, USA) was injected into the largest vein of the CAM to visualize blood vessels, and the CAM was photographed.

Hematoxylin and eosin staining and immunohistochemical staining for αSMA

Chicken embryos were sacrificed and fixed using 4% formaldehyde solution. CAMs topped with tumors were excised and embedded in paraffin, before being sliced perpendicularly into 3 µm sections using a LEICA RM 2155 microtome (Leica, Germany). Standard hematoxylin and eosin (H+E) staining was performed, with H+E stained CAMs with tumors being divided into invasive and non-invasive. Invasion into the CAM was categorized as the destruction of the chorionic epithelium or/and tumor cell invasion into the CAM mesenchyme, tumors that did not invade into the mesenchyme were located on the surface of the CAM, where the integrity of the chorionic epithelium was not disrupted.

To visualize blood vessels in the CAM and quantify angiogenesis, immunohistochemistry for alpha smooth muscle actin (αSMA) was performed. Tissue slices were placed on Superfrost® slides, followed by a standard deparaffinization and rehydration protocol. After the slides were washed three times in distilled water for 1 minute each, epitope retrieval was performed using a high pH epitope retrieval solution (Dako, USA) in a pressure cooker (110°C for 3 min.). The slides were stained using the Thermo Shandon cover plate system (Thermo Fisher Scientific, Inc, USA.). Peroxidase blocking solution (Dako REAL™, Dako, USA) was added, followed by Tween 20 wash buffer for 10 min at room temperature (Dako, USA). Primary antibody anti-αSMA (clone 1A4 Abcam, USA) solution (1:100) was added for incubation for 30 min at room temperature. The slides were washed with Tween 20 wash buffer and the secondary antibody was added (EnVision™ FLEX+ MOUSE (LINKER), Dako, USA), which was followed by the FLEX/HRP (EnVision™ FLEX/HRP, Dako, USA), both incubated for 30 min at room temperature. Slides were then rewashed with Tween 20, and after adding 3,3'diaminobenzidine chromogen (Dako, USA), the slides were washed again. Finally, slides were counterstained using Mayer's hematoxylin solution and covered with coverslips using mounting media (Roti HistoKit, Denmark).

Histomorphometric analysis of the CAM

An Olympus BX43F microscope (Olympus, Corporation, Tokyo, Japan) and an QImaging MicroPublisher 5.0 RTV (Canada) digital camera were used for the morphological evaluation and digital imaging of H+E stained tumors on the CAM. Data comprising the thickness of the CAM (measured at 4x magnification) and the number of blood vessels per constant length from nine experimental groups and four control groups were analyzed. Histomorphometric analysis was performed using the CellSens Dimension 2010 software (version 1.3; Olympus Corporation, Japan).

Statistical analysis

Median values of the number of blood vessels and the thickness of CAM in all investigated groups were compared using a nonparametric Mann-Whitney U-test with GraphPad Prism 6.01 (GraphPad Software, Inc. USA) software. The level of $p<0.05$ was considered to be statistically significant.

Results

Macroscopic evaluation of NCI-H146, A549 and Sk_Lu_1 cell lines' tumors formed on the CAM

Tumors formed from all three tumor cell lines in the control groups attracted newly formed blood vessels (Fig. 1A,E,I), which formed of a varying degree of a "spoke wheel" pattern around the tumors at the EDD12. A "spoke wheel" pattern describes a dense network of blood vessels formed around the tumor and directed towards it. Tumors formed from cells treated with 4 mM NaVP also attracted blood vessels (Fig. 1B,F,J), but did not show signs of tumor regression.

When 6 mM NaVP was applied, a visible change in tumor shape and the number of blood vessels were observed. Tumors formed from A549 cells treated with 6 mM NaVP (Fig. 1C) showed a reduced number of blood vessels. However, the tumor itself continued to grow, forming a round shape, that resembled that of the control group. Tumors formed from Sk_Lu_1 and NCI-H146 cells (Fig. 1G,K) appeared to be at a standstill in response to 6 mM of NaVP. Also, the edges of all evaluated cell lines treated with at 6mM NaVP dose were not as sharp as in the control tumors.

When tumors were treated with 8 mM NaVP (Fig. 1D,H,L), a visible difference in blood vessel numbers was seen. Although large blood vessels surrounded the tumors, small vessels indicating tumor neoangiogenesis were not visible. Tumors derived from both NCI-H146 and Sk_Lu_1 cell lines remained poorly formed, where the number of small blood vessels was reduced (Fig. 1H,L) with no visible vascular network developed around the tumors.

Morphologic evaluation of microscopical changes of the CAM

Tumor behavior and histological changes of CAMs in control and the experimental groups are shown in representative pictures provided in Figure 2. Most

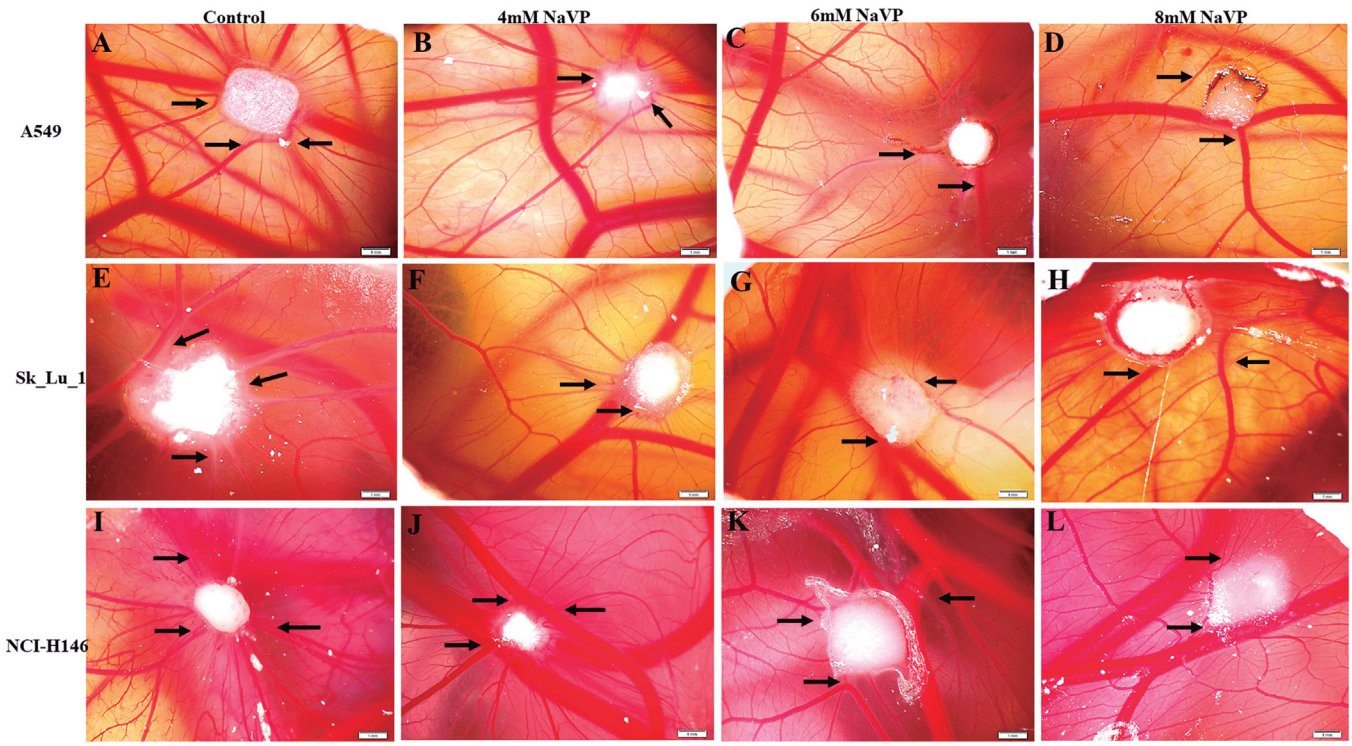

Fig. 1. Representative biomicroscopy *in vivo* images of - NCI-H146, A549 and Sk_Lu_1 cell line tumors treated with different concentrations of sodium valproate (NaVP) versus non-treated (control) group. Images **A-D** show A549 cell line tumors: non-treated **(A)**, 4 mM **(B)**, 6 mM **(C)** and 8 mM **(D)** NaVP treated tumors. Images **E-H** show Sk_Lu_1 cell line tumors: non-treated **(E)**, 4 mM **(F)**, 6 mM **(G)** and 8 mM **(H)** NaVP treated tumors. Images **I-L** show NCI-H146 cell line tumors: non-treated **(I)**, 4 mM **(J)**, 6 mM **(K)** and 8 mM **(L)** NaVP treated tumors. Images taken at EDD12. Black arrows indicate blood vessels. Scale bars: 1 mm.

tumors that were formed from non-treated cell lines penetrated the surface epithelium of the CAM and appeared to be surrounded by mesenchyme, that which had an increased network of blood vessels (Fig. 2A).

Half of the tumors formed from cells treated with 4 mM NaVP remained on the surface of the CAM, with blood vessels that were observed to penetrate the tumor. In all cases the CAM was thickened (Fig. 2B). The image in Figure 2C shows the CAM with a tumor of cells treated with 6mM NaVP, where the effect of the tumor on the CAM was less with a lover: number of blood vessels. Figure 2D shows a CAM with a tumor of cells treated with 8 mM NaVP: tumors appeared flat on the CAM surface, no penetration of blood vessels was observed, the mesenchyme of the CAM itself was not as dense as observed in the groups treated with lower doses of NaVP, and the number of small blood vessels was decreased. Significant differences in the number of blood vessels and thickness of the CAM are described below.

Number of blood vessels in the CAM

The number of blood vessels was counted in the area under the tumor in histological sections stained with H+E. The number of blood vessels in all investigated groups of each cell line was significantly higher than in the control CAM (Fig. 3. asterisk, $p<0.05$). Even though the median value of blood vessels number in the A549 group varied from high (26.0) to low (17.0), no statistically significant difference was found between the control and any other NaVP treated tumors. A significant difference in blood vessel number in the Sk_Lu_1 group was observed comparing the control tumor group with the 6 mM NaVP treated group (Fig. 3. $p=0.037$). NaVP treatment to the cells before grafting significantly diminished the number of blood vessels in the CAMs under the tumors of NCI-H146 cells if compared with the control (Fig. 3. $p<0.001$, $p=0.003$, $p<0.001$ and $p=0.033$ respectively). 6 and 8mM groups expressed the lowest median numbers of blood vessels (7.0 and 7.5,

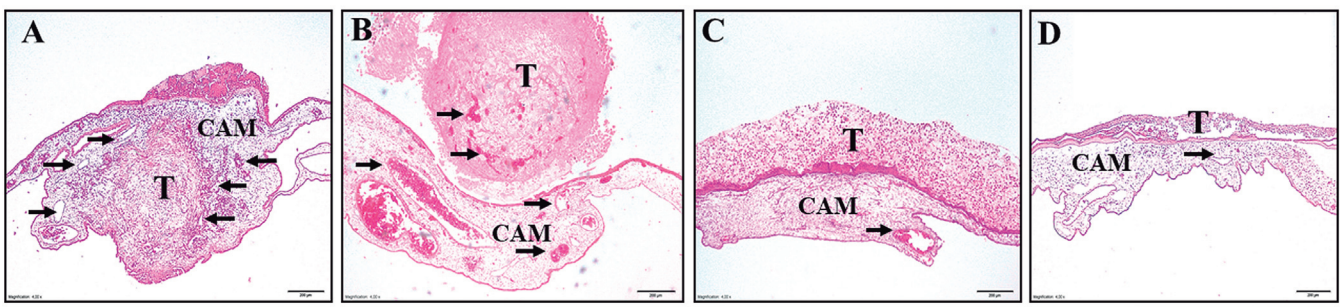

Fig. 2. Tumor invasion and angiogenesis of the CAM. Control group with the tumor and without NaVP treatment **(A)**. 4mM NaVP treated tumor **(B)**, 6mM NaVP treated tumor **(C)**, 8mM NaVP treated tumor **(D)**. T, tumor, CAM, chicken chorioallantoic membrane. Arrows indicate blood vessels. Staining method: H+E, magnification 4x. Scale bars: 200 μm.

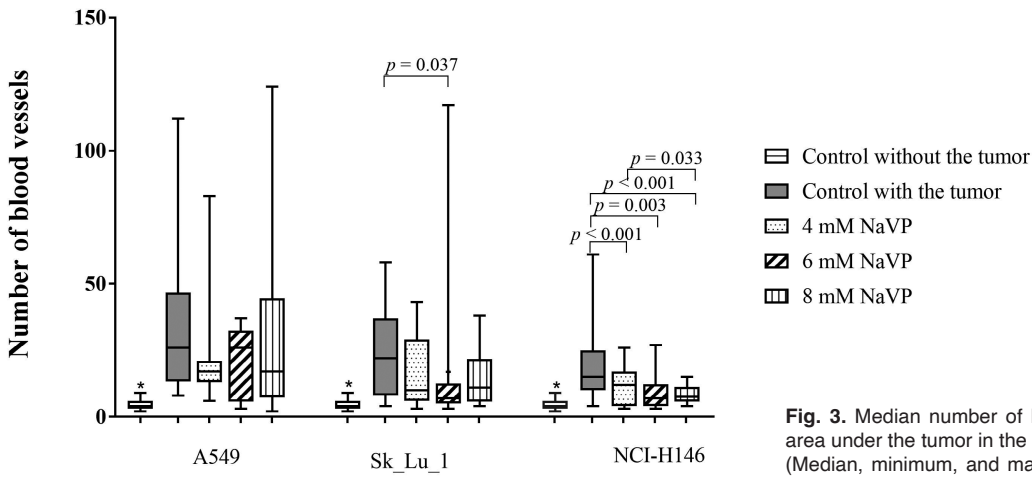

* - $p < 0.05$ with all investigated groups

Fig. 3. Median number of blood vessels in the CAM in the area under the tumor in the control and NaVP treated groups. (Median, minimum, and maximum). Blood vessel number in the control CAMs (without tumor) is significantly lower if compared with all the experimental groups ($p<0.05$).

respectively). The highest median value of the same parameter (15.0) was found in the control tumor group of NCI-H146 cells.

Morphometric evaluation of the thickness of the CAM in A549, Sk_Lu_1 and NCI-H146 groups

CAM thickness in those without tumors was significantly thinner than in all groups with tumors (Fig. 4. $p<0.05$). All the tumors on the CAMs induced the thickening of the mesenchymal layer. The treatment of A549 tumors with 4mM of NaVP did not reduce the thickening of the CAM. CAMs with tumors treated with 6 mM and 8 mM NaVP were significantly thinner compared with non-treated and 4 mM treated groups (Fig. 4. $p<0.001$). CAM in the Sk_Lu_1 c non treated tumor group was significantly thicker than in 4 mM and 6 mM treated groups (Fig. 4. $p<0.001$), but in cases of 8mM NaVP, the CAM was thicker than in 4 mM and 6 mM of NaVP (Fig. 4. $p<0.001$) groups, even when no treatment was applied (Fig. 4. $p<0.02$).

In NCI-H146 tumor experimental groups, the

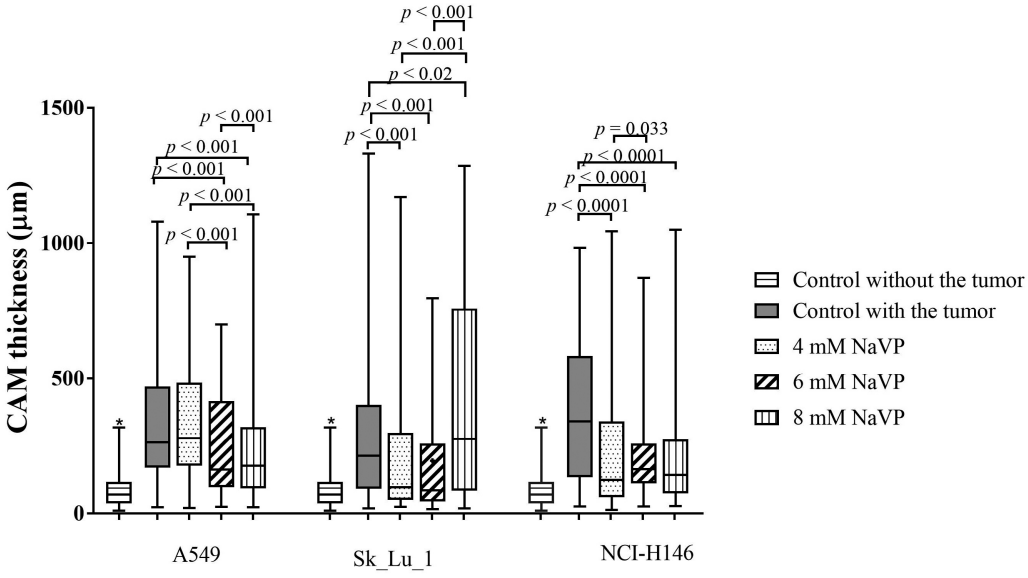

* - $p < 0.05$ with all investigated groups

Fig. 4. CAM thickness in the area under the tumor in the 9 experimental and 4 control groups (median, minimum, and maximum, µm).

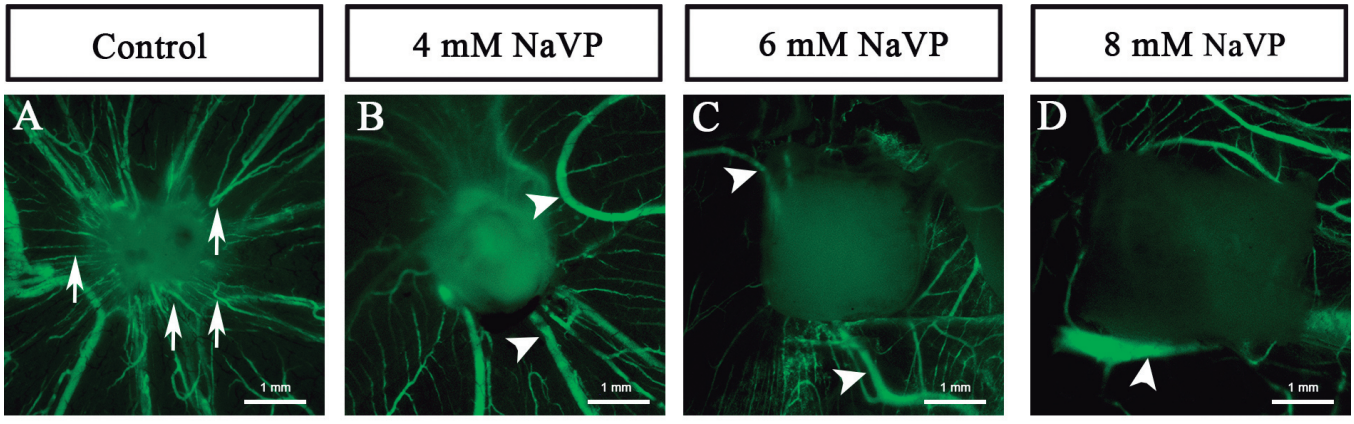

Fig. 5. Representative pictures after fluorescent dextran injection. Non-treated tumor **(A)**, treated with 4 mM **(B)**, treated with 6 mM **(C)**, and treated with 8 mM **(D)** of NaVP. Small blood vessels attracted by the tumor are shown by the arrows and large pre-existing blood vessels are indicated by arrowheads. Photographed at the 12th day of egg incubation. Scale bars: 1 mm.

thickest CAM was in the non-treated group and a significant decrease of the thickness was observed in all NaVP treated groups (Fig. 4. $p<0.0001$), 4 mM and 6 mM NaVP groups differed significantly between each other (Fig. 4. $p=0.033$).

Assessment of the angiogenic response of the CAM with the help of fluorescent dextran after grafting of the tumor

Blood vessels attracted towards the tumor were visualized by introducing fluorescent dextran into the largest vein of the CAM. In the control group of tumor formed from any cell line without NaVP treatment, small blood vessels were seen radially attracted towards the tumor (Fig. 5A, arrows), whereas the tumor itself was round, indicating tumor formation. The tumor with 4 mM of NaVP treatment was still round with larger, pre-existing blood vessels (Fig. 5B, arrowheads). In the 6 mM treated tumor groups only large blood vessels were seen (Fig. 5C, arrowheads) with no sign of small blood vessel branching; also, the tumor did not form a round tumor-like structure and appeared flat. 8 mM of NaVP treated tumor similarly to 6 mM group tumor was seen as flat, and only major, pre-existing blood vessels were visible (Fig. 5D, arrowhead). It is worth noticing that tumors were grafted as a flat structure with the cells infiltrated in the sponge; thus, the more formed the tumor, the more round its structure was, suggesting the idea of tumor malignancy and capability to proliferate. Such a pattern was observed in tumors made from all three cell lines.

αSMA expression in the blood vessels

Blood vessel staining with αSMA showed that we could visibly see a difference in the staining of the endothelium of blood vessels. Immunohistochemical staining of blood vessels with αSMA helped visualize

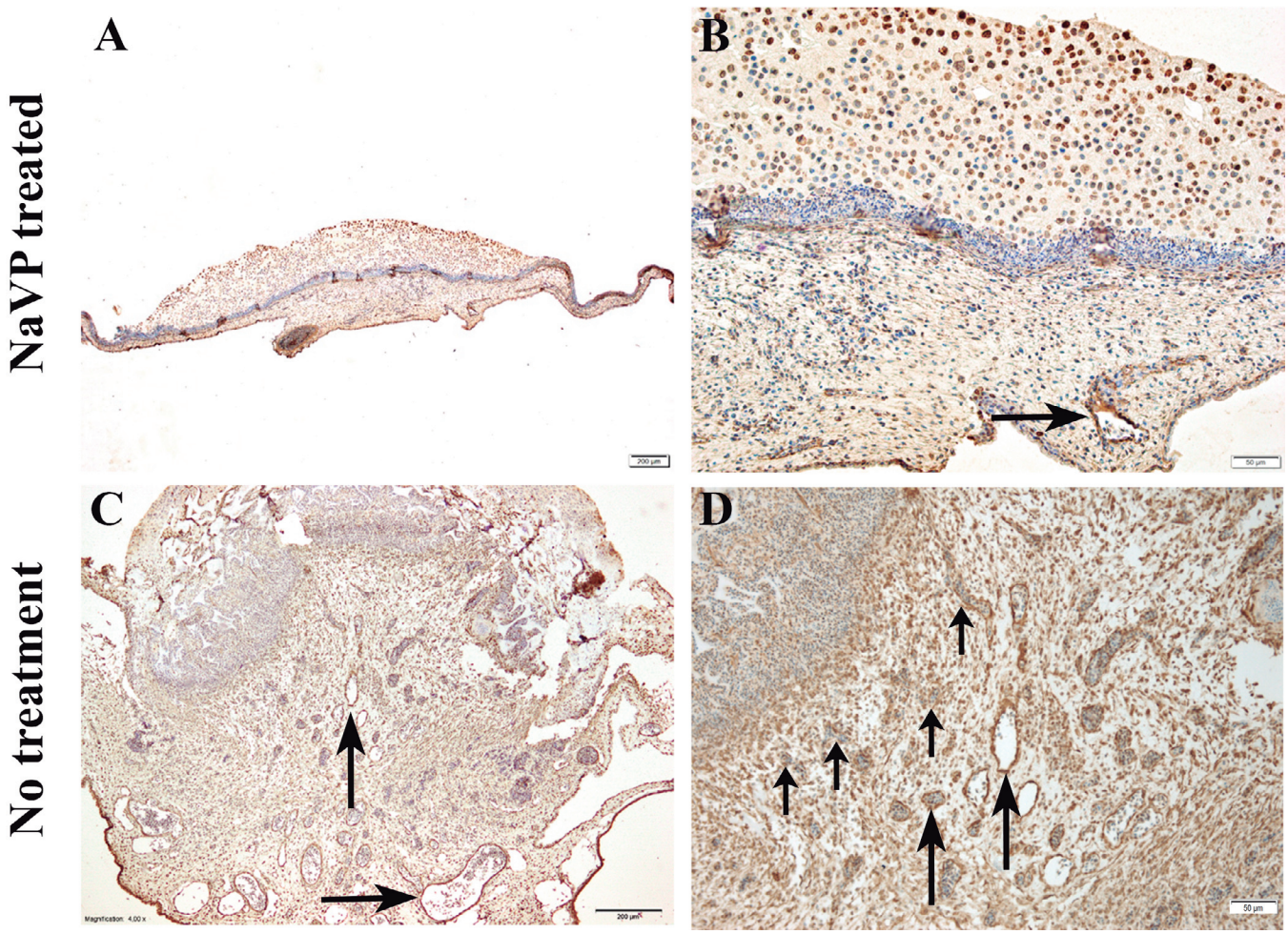

Fig. 6. Immunohistochemical staining with αSMA. NaVP treated group **(A, B)**, Non-treated group **(C, D)**. Small blood vessels indicated by short arrows; long arrows indicate medium size blood vessels. Scale bars: A, C, 200 μm; B, D, 50 μm.

them better, especially the smallest newly formed capillaries. This feature was employed in the counting of blood vessels. In Figure 6, pictures A and B represent a tumor treated with NaVP - the tumor is seen on the top of the CAM with no visible invasion, the epithelium is intact and blood vessels are seen with clear endothelial boundary (Fig. 6B, long arrow) expressing αSMA. Figure 6, pictures C and D show tumors invading CAM with the increased number of blood vessels. In Figure 6, picture C, long arrows show a great amount of large and medium-sized blood vessels clearly expressing αSMA. Picture D is a magnified image showing medium-size blood vessels (Fig. 6D, long arrows) and small blood vessels (Fig. 6D, short arrows) growing towards the tumor.

Tumor invasion into CAM mesenchyme

Tumor invasion into CAM mesenchyme was defined previously (Stakišaitis et al., 2021). A549 cell line tumors without treatment invaded CAM in 91% of all cases. The invasion was observed in fewer cases after applying of 4 mM and 6 mM of NaVP. 6 mM NaVP treatment diminished invasion by up to 50% (p=0.03 compared with the control group, Fig. 7). The frequency of invasion in the 8 mM NaVP treatment group was slightly increased compared with 6 mM group (60%) but was lower than in the control group.

The frequency of Sk_Lu_1 tumor invasion significantly diminished from 86% in the control group to 45% when treated with 4mM. The invasion was detected in only 15% of tumors when 6 mM of NaVP was applied to the cells (p=0.002 and p=0.0002, respectively). After treatment with 8 mM NaVP, invasion to the CAM was even higher (91%) than in the control group (86%). Statistically significant differences were seen comparing 8 mM NaVP group with 6 mM (p=0.0001), and with 4 mM NaVP group (p=0.02).

Invasion in cases of NCI-H146 tumors showed decreased frequency, depending on the NaVP dose. The invasion was the highest (76%) in the control group; it decreased to 50% in the 4 mM NaVP group. Frequency of invasion decreased to the 42.86% in 6 mM group (p=0.04) and to 16.67% in 8 mM NaVP group (p<0.0001), and this decrease was statistically significant. Difference in invasion was significant comparing 4 mM NaVP group with 8 mM NaVP group (p=0.04), Fig. 7.

Discussion

Valproic acid's primary use is as an anti-seizure medication, and it is used in migraine, bipolar, mood, and anxiety disorders. Recent work has also demonstrated its efficacy as adjuvant therapy in HIV, cancer, and neurodegenerative diseases because of its histone deacetylase (HDAC) inhibition property (Rahman and Nguyen, 2021). In the United States, the use of HDAC inhibitors for the treatment of certain cancers has been approved (Zhou et al., 2021). In our investigation in which grafting of an experimental tumor onto the CAM surface was applied, highly increased vascular network, changed direction of CAM blood vessels toward the tumor, even vascularization of an experimental tumor itself was observed. Cancer cells secrete numerous proangiogenic factors: vascular endothelial growth factor, fibroblast growth factor-2, platelet-derived growth factor, platelet-derived endothelial cell growth factor/thymidine phosphorylase, angiopoietins and many others (Marech et al., 2016). These proangiogenic factors stimulate endothelial cells to migrate, proliferate and create new microvessels. Vascular homeostasis is regulated not only by pro-, but also by anti-angiogenic factors. In normal tissues, a balance between tissue factors exists. Induction of new blood vessel formation occurs when pro-angiogenic signaling dominates; this process is called the "angiogenic switch" (Lugano et al., 2020). VEGF is one of the most potent and most investigated inducers of angiogenesis (Ferrara et al., 2003; Kuczynski et al.,

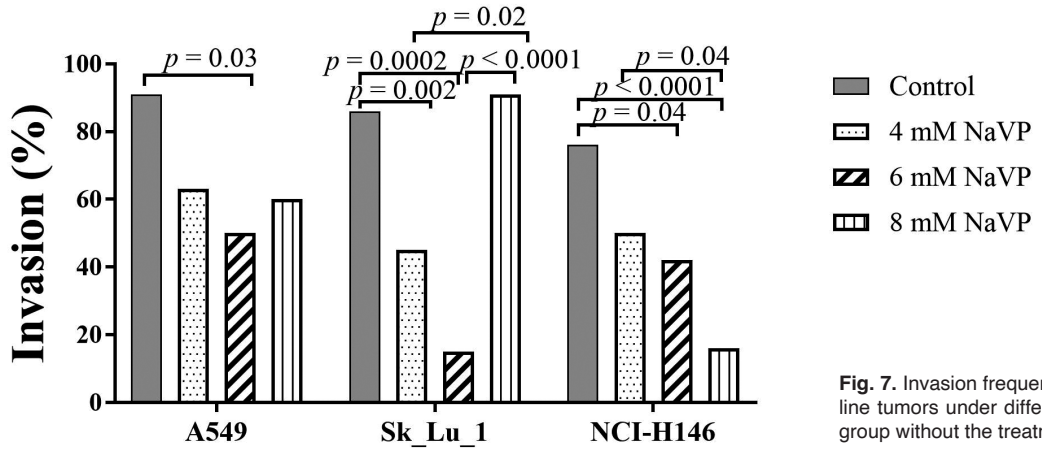

Fig. 7. Invasion frequency % of different lung cancer cell line tumors under different NaVP doses and the control group without the treatment.

2019). Many antiangiogenic strategies in cancer treatment target VEGF (Marech et al., 2016). VEGF and epithelial growth factor inhibitors have become key therapies in lung cancer (Le et al., 2021). In myeloid malignancies NaVP upregulates the expression of anti-angiogenic genes by decreasing the level of proangiogenic factors (Kuendgen and Gattermann, 2007). Our research has shown a decrease in CAM vascularization after applying 4 and 6 mM NaVP. Vascularization was diminished when 8 mM of NaVP was applied in 2 cell line tumors, but in Sk_Lu_1 NSCLC cell line tumors, the vascularization of the CAM was increased. An *in vitro* investigation shows that 1 mM NaVP can significantly inhibit angiogenic potential and VEGF expression in human cervical cancer HeLa and SiHa cells (Zhao et al., 2016). Also, a very recent study revealed that as low as 1.25 mM of NaVP decreases the proliferative properties of endothelial colony-forming cells (Nevo et al., 2020). Our data showed the increase in blood vessel number in the non-treated group versus the treated one and the changes in the staining intensity of αSMA. In a non-treated group, the blood vessels closest to the tumor had less clear αSMA expression. αSMA was very well expressed in large, possibly pre-existing blood vessels if compared with the small blood vessels directed towards the tumor. A quite recent publication found out that the better differentiated a lung cancer was with a higher score of αSMA, a higher survival rate was observed. Poorly differentiated or undifferentiated lung cancers have immature vessels not covered by pericytes or smooth muscle (Usuda et al., 2018). This part of our publication regarding αSMA might suggest either suppressed formation of a new blood vessel or enhanced maturation upon NaVP treatment. Even though the blood vessels were of chicken origin, they may play a role in further investigation of new drugs regarding anti-angiogenesis. Murugavel et al. (2018) *in vitro* experiments have shown that NaVP treatment can directly act on endothelial cells inducing endothelial to mesenchymal transition. Due to the change in the phenotype, the endothelial cells lose their properties, and the mechanism of new blood vessel formation from pre-existing ones is disturbed. They have evident morphological and ultrastructural changes in endothelial cells related to NaVP treatment.

In our work we analyzed cell lines derived from patients of different sexes. A549 and NCI - H146 cell lines were derived from male patients, and the results showed decreased tumor invasion into the CAM, chorioallantoic membrane thickness and a diminished number of blood vessels depending on the NaVP dose. Interesting results were obtained after treating Sk_Lu_1 cells derived from the female patient's tumor with 8 mM NaVP. Tumor invasion, angiogenesis and CAM reaction were diminished when treated with 4 and 6 mM of NaVP. Surprisingly these parameters were elevated when treated with 8 mM NaVP and the invasion reached 91% of cases. These results might be explained in two different ways. First, a more significant amount of Na+ ions may act synergistically with the tumor cells, as reported previously (Grikinienė et al., 2004, 2005). Just as the intracellular ion concentrations can alter cancer cell behavior, the extracellular "ionic tumor microenvironment" can determine how cancer, stromal and infiltrating immune cells behave (Leslie et al., 2019). Preclinical studies show a synergistic effect of sodium dichloroacetate (NaDCA) with the chemotherapy applied in various cancers (Stakišaitis et al., 2019); Stakišaitis et al. discovered that NaDCA impact on U87 MG and PBT24 tumor on proliferating cell nuclear antigen and enhancer of zeste homolog 2 expression in the tumor was different, depending on the NaDCA dose (Stakišaitis et al., 2021). Leslie et al. discovered that at the tissue level, high intracellular [Na+] aids proliferation, migration and invasion of cancer cells and high extracellular [Na+] induces an inflammatory microenvironment that promotes tumor progression (Leslie et al., 2019). Other recent investigations show that sodium influx might be involved in tumor progression (Mao et al., 2019). Voltage-gated sodium channels (VGSCs), transmembrane proteins, are present not only in excitable tissues. These channels participate in the progression of different tumors, including lung cancer (Bon et al., 2016; Mao et al., 2019). Sodium influx into the cancer cell is involved in tumor progression, and it was shown that VGSCs are differently expressed in different lung cancer cells (Roger et al., 2007). High expression of VGSCs in tumors may cause substantial Na^+ influx (Mao et al., 2019). Na^+ influx can also activate voltage-gated calcium channels and intracellular Ca^{2+} concentration increases. Mitochondria rapidly uptake Na^+ and then release Ca^{2+} into the cytosol (Yang et al., 2012). This process is related to the enhanced formation of podosomes/invadopodia and the promotion of invasion (Carrithers et al., 2009). These findings might explain why 8 mM of sodium valproate acts differently and induces Sk_lu_1 tumor growth and invasion. We could not find data about the expression of VGSCs in Sk_Lu_1 and small cell lung cancer. Still, we can speculate that in Sk_Lu_1 cells tumors 8 mM of NaVP concentration was critical to stimulating tumor invasion and angiogenesis progression. Literature sources also claim that VGSCs were not elevated in metastatic A549 cells (Roger et al., 2007). Clinical observations show that some lung cancers are mixed small and non-small lung cancers and some can undergo a transformation from one type to another (Marcoux et al., 2019). Histological transformations of lung cancer cells may develop drug resistance mechanisms, and patients may require a prompt change in clinical management (Rahman and Nguyen, 2021). Our investigation of 3 different lung cancer cell lines shows the different responses to NaVP treatment. Even 2 cell lines obtained from NSCLC patients respond differently to the treatment. Sodium valproate may also affect potassium channels, thereby creating a direct membrane-stabilizing effect (Zhou et al., 2021). A previous study

also shows that NaVP treatment causes a dose-dependent decrease in invasion for all bladder cancer cell lines; however, this effect was not noticed in any of the investigated prostate cancer cell lines (Chen et al., 2006). These findings might demonstrate that the impact of NaVP on invasion is cancer type-specific, and further suggest that the pathways critical to invasion development differ among various cancer types. Wawruszak et al. discovered that the effect of NaVP in monotherapy on induction of apoptosis, inhibition of the cell cycle, EMT, or miRNA pathways do not differ significantly between the histological subtypes of breast cancer cell lines (Wawruszak et al., 2021). However, it has been demonstrated that HER2-overexpressed breast cancer cells are more sensitive to NaVP than HER2-negative; NaVP may synergize with drugs used in the therapy of HER2-overexpressed in breast cancer. Interestingly, a different therapeutic effect was observed in NaVP-combined therapy, depending on the type of breast cancer. It has been demonstrated that the anticancer effect of NaVP, in combination with other active agents, is highly cell-type specific (Wawruszak et al., 2021). Prior studies of HDACIs have focused on cell-growth inhibition and apoptosis induction as primary mechanisms of their anticancer effects (Dragunow et al., 2006), but new experiments showed that sodium valproate might act differently depending on dose and sex and might be cell line-specific (Kavaliauskaitė et al., 2017; Šlekienė et al, 2018, Stakišaitis et al., 2021).

We noted that Sk_Lu_1 cells that responded differently to the 8 mM NaVP treatment were derived from a female patient. Until recently, only minimal attention was paid to the sex of patients who donated their cells to investigate cancer cells from non-reproductive tissues. In a comprehensive investigation by Kim et al. (2019), analyzing their data and in the Cancer Cell line Encyclopedia (database), it was shown that marked differences between cells taken from men and women were observed in liver cancer, but not in colon and lung cancers. The authors studied the sex differences in the expression of EMT associated genes CDH1, VIM, DDR1 and ZEB1. Another group of investigators published data about sex-specific differences in response to the 5-Fluorouracil (5-FU) treatment using human colon cancer cells derived from different sex patients, female and male xenograft mouse models and clinical data for the first time (Lim et al., 2019). They showed that 5-FU-induced cytotoxicity was more significant in female-derived colon cancer cell lines than in male-derived colon cancer cell lines. They also showed that tumor growth inhibition was greater following 5-FU treatment in a female xenograft mouse model than in a male xenograft model. Female colorectal cancer patients treated with 5-FU experienced leukopenia and alopecia more often than male patients. This investigation provided evidence that colon cancer cells themselves "have sex" and respond differently to treatment without any influence of sex hormones (Lim et al., 2019). Mechanism of our current result about the different responses to 8 mM NaVP treatment in the tumor formed from female patient-derived cells compared with the male patient-derived cells requires additional investigation. The sex of the patients cannot be ignored in personalized medicine and preclinical drug investigations with cell cultures and *in vivo* models. Our investigation using the chicken embryo CAM model has shown that NaVP treatment induces a dose-dependent effect on the invasion of the experimental tumors into the CAM mesenchyme and its angiogenic response. Both invasion and angiogenic response depend on the cell line: invasion and angiogenic response of the tumors from A549 and NCI - H146 cell lines responded to the increasing doses from 4 to 8 mM of NaVP, whereas Sk_Lu_1 cells' response was antimigratory and antiangiogenic up to dose 6 mM of NaVP. The dose of 8mM NaVP stimulated invasion and angiogenesis in tumors from Sk_Lu_1 cells.

Acknowledgements. The present study was partially funded by research fund of Lithuanian University of Health Sciences.

A conflict of interest. All authors declare that they have no conflicts of interest.

References

Adelstein D., Tomashefski J., Snow J., Horrigan T. and Hines J. (1986). Mixed small cell and non-small cell lung cancer. Chest 89, 699-704.

Bar J., Ofek E., Barshack I., Gottfried T., Zadok O., Kamer I., Urban D., Perelman M. and Onn A. (2019). Transformation to small cell lung cancer as a mechanism of resistance to immunotherapy in non-small cell lung cancer. Lung Cancer 138, 109-115.

Bon E., Driffort V., Gradek F., Martinez-Caceres C., Anchelin M., Pelegrin P., Cayuela M., Marionneau-Lambot S., Oullier T., Guibon R., Fromont G., Gutierrez-Pajares J., Domingo I., Piver E., Moreau A., Burlaud-Gaillard J., Frank P., Chevalier S., Besson P. and Roger S. (2016). SCN4B acts as a metastasis-suppressor gene preventing hyperactivation of cell migration in breast cancer. Nat. Commun. 7, 13648.

Carmeliet P. (2005). VEGF as a key mediator of angiogenesis in cancer. Oncology 69, 4-10.

Carrithers M., Chatterjee G., Carrithers L., Offoha R., Iheagwara U., Rahner C., Graham M. and Waxman S. (2009). Regulation of podosome formation in macrophages by a splice variant of the sodium channel SCN8A. J. Biol. Chem. 284, 8114-8126.

Chen C., Sung J., Cohen M., Chowdhury W., Sachs M., Li Y., Lakshmanan Y., Yung B., Lupold S. and Rodriguez R. (2006). Valproic acid inhibits invasiveness in bladder cancer but not in prostate cancer cells. J. Pharmacol. Exp. Ther. 319, 533-542.

Dragunow M., Greenwood J., Cameron R., Narayan P., O'Carroll P., Pearson A. and Gibbons H. (2006). Valproic acid induces caspase 3-mediated apoptosis in microglial cells. Neuroscience 140, 1149-1156.

Ferrara N., Gerber H.P. and LeCouter J. (2003). The biology of VEGF and its receptors. Nat. Med. 9, 669-676.

Folkman J. (1971). Tumor angiogenesis: therapeutic implications. N.

Engl. J. Med. 285, 1182-1186.

Folkman J., Merler E., Abernathy C. and Williams G. (1971). Isolation of a tumor factor responsible for angiogenesis. J. Exp. Med. 133, 275-288.

Grikiniene J., Stakisaitis D. and Tschaika M. (2005). Influence of sodium valproate on sodium and chloride urinary excretion in rats, gender differences. Pharmacology 75, 111-115.

Grikinienė J., Volbekas V. and Stakišaitis D. (2004). Gender differences of sodium metabolism and hyponatremia as an adverse drug effect. Medicina 40, 935-942.

Hubaux R., Vandermeers F., Cosse J.P., Crisanti C., Kapoor V., Albelda S. M., Mascaux C., Delvenne P., Hubert P. and Willems L. (2015). Valproic acid improves second-line regimen of small cell lung carcinoma in preclinical models. ERJ Open Res. 1, 1-11.

Iizuka N., Morita A., Kawano C., Mori A., Sakamoto K., Kuroyama M., Ishii M. and Nakahara T. (2018). Anti-angiogenic effects of valproic acid in a mouse model of oxygen-induced retinopathy. J. Pharmacol. Sci. 138, 203-208.

Kalemkerian G.P., Akerley W., Bogner P., Borghaei H., Chow L. Q., Downey R.J., Gandhi L., Ganti A.K.P., Govindan R., Grecula J.C., Hayman J., Heist R.S., Horn L., Jahan T., Koczywas M., Loo B.W., Merritt R.E., Moran C.A., Niell, H.B. and Hughes M. (2013). Small Cell Lung Cancer. J. Natl. Compr. Canc. Netw. 11, 78-98.

Kavaliauskaitė D., Stakišaitis D., Martinkutė J., Šlekienė L., Kazlauskas A., Balnytė I., Lesauskaitė V. and Valančiūtė, A. (2017). The effect of sodium valproate on the glioblastoma U87 cell line tumor development on the chicken embryo chorioallantoic membrane and on EZH2 and p53 expression. Biomed. Res. Int. 1-12.

Kim S., Lee S., Lee E., Lim H., Shin J., Jung J., Kim S. and Moon A. (2019). Sex-biased differences in the correlation between epithelial-to-mesenchymal transition-associated genes in cancer cell lines. Oncol. Lett. 18, 6852-6868.

Kuczynski E., Vermeulen P., Pezzella F., Kerbel R. and Reynolds A. (2019). Vessel co-option in cancer. Nat. Rev. Clin. Oncol. 16, 469-493.

Kuendgen A. and Gattermann N. (2007). Valproic acid for the treatment of myeloid malignancies. Cancer 110, 943-954.

Le X., Nilsson M., Goldman J., Reck M., Nakagawa K., Kato T., Ares L., Frimodt-Moller B., Wolff K., Visseren-Grul C., Heymach J. and Garon E. (2021). Dual EGFR-VEGF pathway inhibition: A promising strategy for patients with EGFR-mutant NSCLC. J. Thorac. Oncol. 16, 205-215.

Leslie T.K., James A.D., Zaccagna F., Grist J.T., Deen S., Kennerley A., Riemer F., Kaggie J.D., Gallagher F.A., Gilbert F.J. and Brackenbury W.J. (2019). Sodium homeostasis in the tumour microenvironment. Biochim. Biophys. Acta Rev. Cancer 1872, 188304.

Lim H., Kim S., Lee E., Lee S., Oh S., Jung J., Kim S. and Moon A. (2019). Sex-dependent adverse drug reactions to 5-fluorouracil in colorectal cancer. Biol. Pharm. Bull. 42, 594-600.

Lucchi M., Mussi A., Fontanini G., Faviana P., Ribechini A. and Angeletti C. A. (2002). Small cell lung carcinoma (SCLC): the angiogenic phenomenon. Eur. J. Cardiothorac. Surg. 21, 1105-1110.

Lugano R., Ramachandran M. and Dimberg A. (2020). Tumor angiogenesis: causes, consequences, challenges and opportunities. Cell. Mol. Life Sci. 77, 1745-1770.

Mangum M., Greco F., Hainsworth J., Hande K. and Johnson D. (1989). Combined small-cell and non-small-cell lung cancer. J. Clin. Oncol. 7, 607-612.

Mao W., Zhang J., Körner H., Jiang Y. and Ying S. (2019). The emerging role of voltage-gated sodium channels in tumor biology. Front. Oncol. 9, 124.

Marcoux N., Gettinger S., O'Kane G., Arbour K., Neal J., Husain H., Evans T., Brahmer J., Muzikansky A., Bonomi P., Del Prete S., Wurtz A., Farago A., Dias-Santagata D., Mino-Kenudson M., Reckamp K., Yu H., Wakelee H., Shepherd F. and Sequist L. (2019). EGFR-Mutant adenocarcinomas that transform to small-cell lung cancer and other neuroendocrine carcinomas: Clinical outcomes. J. Clin. Oncol. 37, 278-285.

Marech I., Leporini C., Ammendola M., Porcelli M., Gadaleta C., Russo E., De Sarro G. and Ranieri G. (2016). Classical and non-classical proangiogenic factors as a target of antiangiogenic therapy in tumor microenvironment. Cancer Lett. 380, 216-226.

Melkonian G., Munoz N., Chung J., Tong C., Marr, R. and Talbot P. (2002). Capillary plexus development in the day five to day six chick chorioallantoic membrane is inhibited by cytochalasin D and suramin. J. Exp. Zool. 292, 241-254.

Michaelis M., Michaelis U., Fleming I., Suhan T., Cinatl J., Blaheta R., Hoffmann K., Kotchetkov R., Busse R., Nau H. and Cinatl J. Jr (2004). Valproic acid inhibits angiogenesis *in vitro* and *in vivo*. Mol. Pharmacol. 65, 520-527.

Murugavel S., Bugyei-Twum A., Matkar P.N., Al-Mubarak H., Chen H.H., Adam M., Jain S., Narang T., Abdin R.M., Qadura M., Connelly K.A., Leong-Poi H. and Singh K.K. (2018). Valproic acid induces endothelial-to-mesenchymal transition-like phenotypic switching. Front. Pharmacol. 9, 737.

Nevo N., Lecourt S., Bièche I., Kucia M., Cras A., Blandinieres A., Vacher S., Gendron N., Guerin G., Ratajczak M. and Smadja D. (2020). Valproic acid decreases endothelial colony forming cells differentiation and induces endothelial-to-mesenchymal transition-like process. Stem. Cell. Rev. Rep. 16, 357-368.

Oser M.G., Niederst M.J., Sequist L.V. and Engelman J.A. (2015). Transformation from non-small-cell lung cancer to small-cell lung cancer: molecular drivers and cells of origin. Lancet Oncol. 16, e165-172.

Rahman M. and Nguyen H. (2021). Valproic acid. Encyclopedia of toxicology. Third Edition. pp 905-908.

Roger S., Rollin J., Barascu A., Besson P., Raynal P., Iochmann S., Lei M., Bougnoux P., Gruel Y. and Le Guennec J.Y. (2007). Voltage-gated sodium channels potentiate the invasive capacities of human non-small-cell lung cancer cell lines. Int. J. Biochem. Cell. Biol. 39, 774-786.

Schmitd L.B., Liu M., Scanlon C.S., Banerjee R. and D'Silva N.J. (2019). The chick chorioallantoic membrane *in vivo* model to assess perineural invasion in head and neck cancer. J. Vis. Exp. 148, e59296

Sequist L.V., Waltman B.A., Dias-Santagata D., Digumarthy S., Turke A.B., Fidias P., Bergethon K., Shaw A.T., Gettinger S., Cosper A.K., Akhavanfard S., Heist R.S., Temel J., Christensen J.G., Wain J.C., Lynch T.J., Vernovsky K., Mark E.J., Lanuti M., Iafrate A.J., Mino-Kenudson M. and Engelman J.A. (2011). Genotypic and histological evolution of lung cancers acquiring resistance to EGFR inhibitors. Sci. Transl. Med. 3, 75ra26.

Šlekienė L., Stakišaitis D., Balnytė I. and Valančiūtė A. (2018). Sodium valproate inhibits small cell Lung cancer tumor growth on the chicken embryo chorioallantoic membrane and reduces the p53 and EZH2 expression. Dose Response 16, 1559325818772486.

Stakišaitis D, Juknevičienė M., Damanskienė E., Valančiūtė A., Balnytė I. and Alonso M. (2019). The importance of gender-related

anticancer research on mitochondrial regulator sodium dichloroacetate in preclinical studies *in vivo*. Cancers 11, 1210.

Stakišaitis D., Damanskienė E., Juknevičienė M., Alonso M., Valančiūtė A., Ročka S. and Balnytė I. (2021). The effectiveness of dichloroacetate on human glioblastoma xenograft growth depends on Naþ and Mg2þ cations. Dose Response 19, 1559325821990166.

Usuda K., Iwai S., Funasaki A., Sekimura A., Motono N., Ueda Y., Shimazaki M. and Uramoto H. (2018). Expression and prognostic impact of VEGF, CD31 and αSMA in resected primary lung cancers. Anticancer Res. 38, 4057-4063.

Vasudev N. and Reynolds A. (2014). Anti-angiogenic therapy for cancer: current progress, unresolved questions and future directions. Angiogenesis 17, 471-494.

Vos T., Allen C., Arora M., Barber R.M., Bhutta Z.A., Brown A., Carter A., Casey D.C., Charlson F.J., Chen A.Z., Coggeshall M., Cornaby L., Dandona L., Dicker D.J., Dilegge T., Erskine H.E., Ferrari A.J., Fitzmaurice C., Fleming T. and Murray C.J.L. (2016). Global, regional, and national incidence, prevalence, and years lived with disability for 310 diseases and injuries, 1990-2015: a systematic analysis for the Global Burden of Disease Study 2015. Lancet 388, 1545-1602.

Wawruszak A., Halasa M., Okon E., Kukula-Koch W. and Stepulak A. (2021). Valproic acid and breast cancer: State of the art in 2021. Cancers (Basel) 13, 3409.

Yang M., Kozminski D., Wold L., Modak R., Calhoun J., Isom L. and Brackenbury W. (2012). Therapeutic potential for phenytoin: targeting Na(v)1.5 sodium channels to reduce migration and invasion in metastatic breast cancer. Breast Cancer Res. Treat. 134, 603-615.

Yu H., Arcila M., Rekhtman N., Sima C., Zakowski M., Pao W., Kris M., Miller W., Ladanyi M. and Riely G. (2013). Analysis of tumor specimens at the time of acquired resistance to EGFR-TKI therapy in 155 patients with EGFR-mutant lung cancers. Clin. Cancer Res. 19, 2240-2247.

Zhao Y., You W., Zheng J., Chi Y., Tang W. and Du R. (2016). Valproic acid inhibits the angiogenic potential of cervical cancer cells via HIF-1α/VEGF signals. Clin. Transl. Oncol. 18, 1123-1130.

Zhou M., Yuan M., Zhang M., Lei C., Aras O., Zhang X. and An F. (2021). Combining histone deacetylase inhibitors (HDACis) with other therapies for cancer therapy. Eur. J. Med. Chem. 226. 113825.

Accepted June 15, 2022